Submitted to ADVANCED MATERIALS
DOI: 10.1002/adma.((please add manuscript number))
Article type: Communication

Acoustic enhancement of polymer / ZnO nanorod photovoltaic device performance

*Safa Shoaee, Joe Briscoe, James R Durrant and Steve Dunn**

Safa Shoaee, James R Durrant
Centre for Plastic Electronics, Department of Chemistry, Imperial College London, London SW7 2AZ, United Kingdom
E-mail: j.durrant@imperial.ac.uk
Joe Briscoe, Steve Dunn
Centre for Materials Research, School of Engineering and Materials, Queen Mary University of London, E1 4NS, United Kingdom
E-mail: s.c.dunn@qmul.ac.uk

Keywords: solar cell, piezoelectric, hybrid, zinc oxide, P3HT

Photovoltaic (PV) devices based on conjugated polymers and nanostructured metal oxides have been widely studied as a hybrid inorganic/organic approach to solar energy conversion.[1–7] A large source of loss in this type of device is non-radiative recombination of the photogenerated charge carriers. Therefore, strategies to reduce this recombination have the potential to significantly increase device efficiency.[8] If utilised effectively, the electric field generated by a non-centrosymmetric crystal has the potential to modulate the performance of optoelectronic devices.[8] In this paper, we show for the first time that acoustic vibration can be utilised to enhance significantly photocurrent generation and solar to electric power conversion efficiency (PCE_{S-E}) of an optoelectronic device comprising a hybrid organic-inorganic photovoltaic cell of poly(3-hexylthiophene) (P3HT) and ZnO nanorods. The application of modest external vibration (10 kHz at 75dB, equivalent to a loud office environment) is shown to cause a 45% increase in device efficiency, correlated with a 3-fold increase in charge carrier lifetime. By identifying reduced recombination as the origin of the performance enhancement, and with comparison to control systems we propose a mechanism based on the piezoelectric properties of ZnO nanorods as the source of the enhancement. This

study thus demonstrates a novel approach to enhancing the photovoltaic energy conversion applicable to environments where high levels of ambient vibrations are present such as vehicles, roof-mounted machinery and defence applications. In addition, it indicates that the piezoelectric properties of materials should be taken into consideration during testing of photovoltaic devices.

Nanostructured materials are currently attracting extensive attention to reduce the cost and/or enhance the efficiency of photovoltaic solar energy conversion.[9–12] Such nanostructuring is typically employed to reduce the distance the excited states or charge carriers must travel to reach a device interface. Hybrid structures of nanostructured metal oxides and conjugated polymers combine the structural control offered by the inorganic scaffold with the ease of processing and strong optical light absorption of semiconducting polymers. Efforts to improve device performance have focused on the fabrication of inorganic nanostructured materials,[3] the modification of the interface between polymer and the metal electrode[3] and band offset engineering.[6] One of the most widely studied inorganic semiconductors for such hybrid devices is zinc oxide (ZnO);[1,3,5] it benefits from a wide band gap, good carrier mobility,[13] a large variety of morphologies,[14,15] and, of particular interest for this manuscript, piezoelectric behaviour.[16] A piezoelectric material produces a polarisation and associated electric field upon application of acoustic or mechanical stress, which can be employed to convert kinetic energy to electrical energy.[17–21] If utilised effectively, this electric field has the potential to modulate the performance of optoelectronic devices.[8,22–24]

Control of the materials morphology and nanostructure is well known as a key determinant of device performance.[3,7,13] For ZnO, there are many examples of different kinds of nanostructures that have been successfully characterized[25] and integrated into optoelectronic devices:[5,26] nanoparticles, nanorods, nanotubes and nanoribbons being the most common.[15] For the study herein, ZnO nanorods interfaced with the most widely used p-type polymer

donor, poly(3-hexylthiophene) (P3HT), provides a well-defined model system with which to study the impact of ZnO aspect ratio and external vibrations on photovoltaic device performance.

It has previously been shown that in P3HT/ZnO nanorod array PVs, photocurrent improves with rod length.[5] Other alternative ZnO PV's architectures have also demonstrated that there is an optimal length of nanorods and explained this is terms of carrier mobility and photon capture.[27] In parallel with such studies, nanostructured ZnO materials have been shown to exhibit a variety of vibrational energy harvesting capabilities.[18,20] However, studies employing piezoelectric effects to enhance the performance of photovoltaic devices have been very limited to date. Such studies have shown parallel piezoelectric and photovoltaic device performance where small piezoelectric voltage outputs are added to the photovoltage but lead to negligible enhancement in photovoltaic current generation and solar power conversion efficiency under simulated solar irradiation (AM1.5 ~100 mW cm^{-2}).[28–31]

In this article we present data that demonstrate, for the first time, that applied acoustic vibration can lead to significant enhancements in device solar to electric power conversion efficiency. We demonstrate that the enhancement originates from a reduction in the charge carrier recombination and propose a mechanism whereby this enhancement can be achieved by the presence of alternating electric fields at the surface of the ZnO nanorods due to a piezoelectric effect. In contrast to previous work, the piezoelectric effect is thus used to directly enhance photovoltaic device efficiency rather than as an additive combination of two separate processes.

ZnO nanorods were grown on ZnO-seeded conductive glass substrates using an aqueous chemical method.[32] Five different sized nanorods were grown by varying the reactant concentrations and reaction time. The ZnO nanorods form homogenous and well-oriented hexagonal shape with aspect ratios of A:38, B:30, C:20, D:19, E:5, as shown in **Figure 1**. Aspect ratios were calculated by measuring the average length and diameter of the nanorods

from cross-section SEM images (Figure S1). Further details of synthesis conditions and materials characterisation are given in experimental section. P3HT was deposited by a combined dip and spin coating methodology shown previously to yield efficient device performance.[3] As previously,[3] this method led to good penetration of the P3HT between the ZnO nanorods (Figure S2), leading to an intimate P3HT/ZnO layer with a thickness equal to the nanorod length (See Table S1), and a capping layer of P3HT above the rods of 300-500 nm, which was kept constant by using a constant P3HT concentration and spin speed.[5] This prevented contact between the ZnO and the Au top electrode (which was evaporated to complete the device) by effectively acting as an electron blocking layer.[5]

In **Figure 2**a current density-voltage (J-V) curves of ITO/ZnO seed layer/ZnO(X)/P3HT/Au devices, under A.M. 1.5 illumination, are shown for several different nanorod aspect ratios. It is apparent that increasing nanorod aspect ratio results in a significant enhancement in device performance. The highest photovoltaic power conversion efficiency is achieved with the highest aspect ratio (ZnO(A)), with a significant increase in the short-circuit current density (J_{sc}) and a slight increase in the open-circuit voltage (V_{oc}). An increase in J_{sc} as a function of rod length has recently been reported for analogous devices.[5] This could partly be accounted for by the increased interface area of P3HT/ZnO(X) (See Table S1),[5] although the photocurrent correlated more closely with aspect ratio than interface area. Changes in V_{oc} may be partly accounted for by strain-induced band shifts.[33] We note that, as typical of hybrid PV cells, the device fill factors were largely limited by dark shunt resistances.

To understand the origin of the increases in device photocurrent and PCE_{S-E} with changes in ZnO nanorod aspect ratio, the underlying photoinduced processes determining photovoltaic device function were investigated by employing transient absorption spectroscopy to monitor the photoinduced absorption of the P3HT cations. We have previously demonstrated that such nano-millisecond transient absorption spectroscopy can be an effective assay of the yield of

dissociated charge carriers and their recombination dynamics in P3HT/ZnO blend films.[3] Typical transient absorption data for P3HT/ZnO films analogous to those employed for device fabrication are shown in Figure 2b. Data were collected at a probe wavelength 980 nm, assigned as previously[34] to the absorption maxima of $P3HT^+$ polarons (See Figure S3). In all blends, the transients were oxygen-independent, consistent with their assignment to polaron rather than triplet absorption, and exhibited approximately exponential decay dynamics. Transient data scaled approximately linearly with excitation density, and were normalised for small changes in P3HT absorption at the excitation wavelength of 500 nm. Control data on neat P3HT and neat ZnO nanorod films gave negligible transient signals on the timescales studied. Figure 2b shows a clear trend in the decay times of the transients with ZnO nanorod aspect ratio, with the decay lifetime increasing from 60 to 270 μs as the aspect ratio is increased. These decays are assigned as previously[3] to non-geminate recombination of dissociated charge carriers – we therefore conclude that increasing rod aspect ratio results in a 4.5 fold decrease in this non-geminate recombination rate.

The observed increase in carrier lifetime with nanorod aspect ratio is unexpected.[35] The increase in interfacial surface area with increased aspect ratio would be expected to accelerate non-geminate recombination. This has been reported previously in analogous studies on the effect of annealing on nano-morphology and recombination dynamics in P3HT:PCBM films.[36] The observation herein of the opposite trend is striking, and suggests the different aspect ratio rods interact differently with the P3HT exciton. Due to identical processing the surfaces of the different aspect ratio rods should not vary, and aspect ratio differences should only affect the mechanical properties of the nanorods.

To further investigate possible variations in the mechanical response, acoustic vibration was applied to the samples through a loudspeaker (75 dB at 1-50 kHz). We observed an enhancement in device performance of each solar cell when under external vibration (**Figure 3**a). For all devices V_{oc} increased by 10-50 mV, and J_{sc} increased by up to 2.3 $mAcm^{-2}$. These

enhancements were frequency-dependent, with a large increase around 10 kHz (Figure S4). This is in the range of resonance frequencies for ZnO nanorods measured previously,[37] which suggests that the coupling of the vibration to the ZnO nanorods is the source of the enhancement. An analogous enhancement in photocurrent generation was also observed for polymer/ZnO devices employing an alternative donor polymer PCDTBT (Figure S5), demonstrating that the enhancement is not specific to P3HT. Control P3HT:PCBM bulk heterojunction devices displayed no dependence upon the application of external vibration (Figure S6 and S7). Similarly, control experiments employing P3HT:PCBM bulk heterojunctions deposited onto ZnO nanorods yielded no significant dependence of photocurrent generation upon external vibration (Figure S8). This device is morphologically very similar to the P3HT/ZnO and PCTBT/ZnO devices with the polymer layers deposited over the nanorods, but the charge separation and non-geminate recombination occurs at the P3HT:PCBM interface, rather than the polymer/ZnO interface. These results thus suggest that the observed enhancement in device performance under acoustic stress results is obtained in devices where photoinduced charge separation occurs at a polymer/ZnO nanorod heterojunction. An increase in open-circuit voltage in the order of 18 mV has been previously reported for analogous ZnO photovoltaic devices subjected to applied vibration, ascribed to the addition of the piezoelectrically generated voltage to the photovoltage.[28,29] However the significant increase in both photovoltage and photocurrent and consequently the increase in the overall solar to electric power conversion efficiency has not been reported previously. For our highest aspect ratio device, the application of external vibration resulted in the PCE_{S-E} increasing from 1.35 to 1.75%.

To verify the validity of the data under external vibration and check their performance and stability, devices were re-tested after the vibration tests had been performed; the cells under study always went back to their original (no external vibration) JV curve after removing the applied vibration. This indicated that the performance enhancement only lasted during the

application of vibration, and that the application of vibration did not adversely affect the stability of the devices. It should be noted that the cells were un-encapsulated devices, and therefore degraded under prolonged air exposure.

Transient absorption data were also measured under applied acoustic vibration. For all blends studied, this applied stress resulted in a substantial increase in the charge carrier lifetime. Typical data are shown in Figure 3b for the highest aspect ratio rods (exhibiting the largest effect), which shows an increase in carrier lifetime from 0.34 ms to 0.88 ms under applied stress (see Figure S9 for the full data set). Analogous data were obtained for PCDTBT/ZnO junctions whilst control data on P3HT:PCBM blend films displayed no such dependence on applied stress (Figure S5 and S7). These data provide clear strong evidence that acoustic vibrations can substantially enhance the charge carrier lifetime in polymer/ZnO nanorod films.

The transient absorption data in Figure 2b and 3b show increases by up to 50% in initial signal amplitude both with increased nanorod aspect ratio and applied strain. This is indicative of either increased charge separation efficiency, or reduced recombination losses on timescales faster than our time resolution (~100 ns). In order to investigate this issue further, photoluminescence data were collected to assay the extent of P3HT emission quenching relative to a neat P3HT film (see Figure S10). For all the P3HT/ZnO films studied, P3HT emission was observed to be strongly quenched, with the quenching efficiency increasing modestly with decreasing aspect ratio from ~ 90 to 98 %. These data suggest that neither variations in P3HT exciton diffusion nor exciton separation at the P3HT/ZnO interface are likely to strongly impact upon the trends in charge carrier yields and photocurrent densities we report. As such, we assign the increased photovoltaic device performances with both aspect ratio and acoustic strain that we observe herein to reduced losses due to charge carrier recombination (non-geminate and potentially geminate), as indicated by the transient absorption data shown in Figure 2b and 3b. Our transient absorption data indicate that the

observed increases in charge carrier signal amplitudes and lifetimes (50% and three-fold increases respectively) are large enough to explain the increases in photovoltaic device efficiency with nanorod aspect ratio and acoustic strain shown in Figure 2a and 3a.

We now discuss possible mechanisms within our model PV system that could be affected by the nanorod aspect ratio and acoustic vibration leading to enhanced carrier lifetime and device performance. There are a number of effects that can result from subjecting the devices to acoustic vibrations. It is possible that the applied vibration and additional freedom of movement could improve the interfacial contact between the ZnO and P3HT leading to increased device efficiency. However, this would be expected to increase P3HT exciton quenching rather than retard recombination, in direct contrast to our transient absorption and photoluminescence quenching data. Additionally, the acoustic vibrations could induce local heating in the materials. However, local heating would be expected to accelerate recombination losses and reduce cell voltage, again in contrast to our experimental observations. Furthermore, the acoustic vibration induced performance enhancement we report is fully reversible, indicating the acoustic vibrations do not result in any irreversible change in materials structure. Our comparison of three different junctions: P3HT/ZnO, PCDTBT/ZnO and P3HT:PCBM clearly indicates that observed PV efficiency enhancement under acoustic strain originates from the ZnO nanorods and specifically their mechanical response to both ambient and applied vibrations. Additionally, the enhancement does not occur in P3HT:PCBM/ZnO films, where the charge separation and recombination interface is between the P3HT and PCBM, not at the ZnO interface. Thus the enhancement only occurs in configurations where the charge separation interface is at the ZnO surface, which implies that the effect results form a change in the properties of this interface brought about by the acoustic vibrations.

As discussed, ZnO is a piezoelectric material and therefore develops a polarisation and associated surface charge upon the application of external stress. We have shown previously

that a ZnO nanorod-polymer system can develop an external voltage due to the piezoelectric effect when subjected to acoustic vibration, which increased with applied frequency and the aspect ratio or length of the rods.[19] In the data reported herein the direct piezoelectric power output from the devices when subjected to external vibration in the dark was much smaller than the vibration-induced increase in solar to electric power output observed under solar irradiation, indicating that this increase cannot be a simple additive effect, in contrast to previous reports.[28,31] As such, we therefore suggest that the enhanced photovoltaic performance reported herein originates from the impact of piezoelectrically-induced electric fields on the charge photogeneration and recombination dynamics of the device.

Figure 4 shows a suggested mechanism by which the piezoelectric polarisation could enhance the lifetimes of photogenerated charge carriers in the hybrid polymer/ZnO nanorod devices studied here, and thereby increase device solar to electric power conversion efficiency. As discussed, when ZnO nanorods experience strain due to vibrations, an alternating polarisation will develop across these nanorods. The electric fields associated with this polarisation can be expected to extend into both the ZnO and polymer components. Such fields in piezo- and ferroelectric are well-known to strongly influence free carriers at the interface, which leads to screening of the polarisation as the carriers rearrange.[8,16,19] As the nanorods vibrate, the surface will fluctuate between positive and negative polarisations (Figure 4). These polarisations will provide an oscillating modulation of the energetics of exciton separation at the P3HT/ZnO interface. As this effect should alternate between a positive and negative contribution, and is in any case likely to be small compared to the large energy offset driving exciton separation (~1 eV), it is unlikely to be the origin of observed performance enhancement. This is in agreement with our spectroscopic data which indicates that the performance enhancement does not derive from increased exciton separation. However, after exciton separation, depending upon the polarity of the ZnO polarisation relative to the polymer/ZnO interface, the resultant electric fields will either drive separated

electrons in ZnO (Figure 4c) or positive polarons in P3HT (figure 4b) away from the P3HT/ZnO interface. Importantly, the opposite carrier is already at the junction, and thus cannot be forced closer by the electric field, nor can it cross the junction due to the energy barrier. Therefore, in either case, these piezoelectric-induced fields will increase the spatial separation of photogenerated electrons and holes and thereby reduce charge carrier recombination, in agreement with our transient kinetic data (Figure 3b). This model therefore accounts for the observation that the efficiency enhancement occurs due to a reduction in charge carrier recombination rather than due to enhanced exciton separation. We note the inversion of field orientation with acoustic oscillations would result in oscillating enhancement and suppression of exciton separation, likely to cancel out even if this is significant effect. A comparable model can used to explain the enhancement of device performance with nanorod aspect ratio even in the absence of applied acoustic strain – the higher aspect ratio rods can be expected to bend to a greater degree under the ambient vibrations, increasing piezoelectric polarisation and thus retarding recombination losses, consistent with our experimental observations. Clearly the study we have reported herein is limited scope, and other effects may also contribute to the reported efficiency enhancements. Nevertheless the model illustrated in Figure 4 is in good qualitative agreement with our transient kinetic and device data, and illustrates the potential for oscillating piezoelectric effects to enhance photovoltaic device performance.

On a lighter note, the response of the devices to a variety of acoustic conditions was investigated by playing a variety of different types of music during testing, rather than single frequency signals as used above. It was found that the efficiency enhancement was most pronounced for pop rather than classical music, most probably due to the increased amplitudes of higher frequencies typically present in electronically synthesised music.

In summary, we have shown the solar to electric power conversion efficiency of P3HT/ZnO hybrid solar cells can be substantially enhanced both by increasing ZnO nanorod

aspect ratio and the application of modest acoustic vibration. This enhancement has been shown using transient absorption studies to originate from reduced charge carrier recombination losses, which have been explained via the piezoelectric effect in the ZnO nanorods. The proposed model is consistent with the lack of enhancement in control systems. We envisage these effects may also be relevant to other photovoltaic device structures which employ high aspect ratio nanostructures capable of piezoelectric effects. This conclusion is supported by the analogous results for the PCDTBT/ZnO system. This discovery may lead to applications where photovoltaic, as well as other optoelectronic devices such as sensors, could be sited in areas of high ambient vibrations such as on air-conditioning units on roofs, on vehicles or in defence applications to access this significant efficiency enhancement.

Experimental Section

ZnO fabrication: ZnO nanorods were grown on ITO-coated glass substrates seeded with a sputtered ZnO film. Seeded substrates were suspended in solutions of zinc nitrate and hexamethylenetetramine (HMT) and heated to 90 °C to grow the ZnO nanorods. Five different aspect ratios were produced by using different concentrations of reactants and different total reaction times. Depending on the reactant concentration the reactants became depleted after 2.5-4 hours after which the substrates were placed in a fresh solution. The following reactant concentrations, times and repeats were used for each type of rod: A, 25 mM HMT, 15 mM zinc nitrate, 8 repeats of 4 hours; B, 25 mM HMT and 15 mM zinc nitrate, 4 repeats of 4 hours; C, 25 mM HMT and zinc nitrate, 6 repeats of 2.5 hours; D, 25 mM HMT and zinc nitrate, 3 repeats of 2.5 hours; E, 0.1 M HMT and zinc nitrate, one 4 hour reaction. After growth the ZnO nanorods were annealed in air at 400 °C for 1 hour. Scanning electron microscopy (SEM) micrographs of ZnO nanorods were recorded using an FEI Inspect-F SFEG SEM.

Device fabrication: ZnO nanorod samples were first immersed overnight in a solution of polymer in chlorobenzene (2 g/l). The dip coated films were then dried by N_2 gas. Subsequently a polymer layer was spin coated from chlorobenzene (45 g/l) at 1100 rpm. Finally gold contacts (50 nm) were deposited by evaporation.

Transient absorption decays were measured by exciting the sample film under a nitrogen (and oxygen) atmosphere, excitation pulses were generated with a commercially available optical parametric oscillator (Oppolette) pumped by Nd:YAG laser (Lambda Photometrics). The excitation wavelength used was 500 nm for P3HT and 550 nm for PCDTBT blend films, with a pump intensity of 0.4 - 20 $\mu J.cm^{-2}$ and a repetition frequency of 20 Hz. For 1 μs – 1 ms timescale, a 100 W quartz halogen lamp (Bentham, IL 1) with a stabilised power supply (Bentham, 605) was used as a probe light source (980 nm). The signal from the photodiode was pre-amplified and sent to the main amplification system with an electronic band-pass filter (Costronics Electronics). The amplified signal was collected with a digital oscilloscope (Tektronics, TDS220), which was synchronised with a trigger signal of the pump laser pulse from a photodiode (Thorlabs Inc., DET210). To reduce stray light, scattered light and sample emission, two monochromators and appropriate optical cut-off filters were placed before and after the sample.

For all devices, the external control vibration was applied at a fixed distance, through a loud speaker at 75 dB, with frequencies ranging between 1 – 50 kHz.

Supporting Information

Supporting Information is available online from the Wiley Online Library or from the author.

Acknowledgements

The authors are grateful to the Leverhulme Trust and EPSRC (projects EP/J500021/1 and EP/G037515/1)for funding, Simon Dowland for useful discussions and Rory McFarlane for advice on the frequency content of music sources.

Received: ((will be filled in by the editorial staff))
Revised: ((will be filled in by the editorial staff))
Published online: ((will be filled in by the editorial staff))

[1] S. D. Oosterhout, M. M. Wienk, S. S. van Bavel, R. Thiedmann, L. J. A. Koster, J. Gilot, J. Loos, V. Schmidt, R. A. J. Janssen, *Nat. Mater.* **2009**, *8*, 818–824.

[2] L. Zhao, Z. Lin, *Adv. Mater.* **2012**, *24*, 4353–4368.

[3] P. Ravirajan, A. M. Peiró, M. K. Nazeeruddin, M. Graetzel, D. D. C. Bradley, J. R. Durrant, J. Nelson, *J. Phys. Chem. B* **2006**, *110*, 7635–7639.

[4] I. Gonzalez-Valls, M. Lira-Cantu, *Energy Environ. Sci.* **2009**, *2*, 19–34.

[5] L. Baeten, B. Conings, H.-G. Boyen, J. D'Haen, A. Hardy, M. D'Olieslaeger, J. V Manca, M. K. Van Bael, *Adv. Mater.* **2011**, *23*, 2802–2805.

[6] D. C. Olson, S. E. Shaheen, M. S. White, W. J. Mitchell, M. F. A. M. van Hest, R. T. Collins, D. S. Ginley, *Adv. Func. Mater.* **2007**, *17*, 264–269.

[7] J. Boucle, P. Ravirajan, J. Nelson, *J. Mater. Chem.* **2007**, *17*, 3141–3153.

[8] Y. Yuan, T. J. Reece, P. Sharma, S. Poddar, S. Ducharme, A. Gruverman, Y. Yang, J. Huang, *Nat. Mater.* **2011**, *10*, 296–302.

[9] I. Chung, B. Lee, J. He, R. P. H. Chang, M. G. Kanatzidis, *Nature* **2012**, *485*, 486–489.

[10] B. Tian, X. Zheng, T. J. Kempa, Y. Fang, N. Yu, G. Yu, J. Huang, C. M. Lieber, *Nature* **2007**, *449*, 885–889.

[11] N. S. Lewis, *Sci.* **2007**, *315* , 798–801.

[12] J. Tang, K. W. Kemp, S. Hoogland, K. S. Jeong, H. Liu, L. Levina, M. Furukawa, X. Wang, R. Debnath, D. Cha, K. W. Chou, A. Fischer, A. Amassian, J. B. Asbury, E. H. Sargent, *Nat. Mater.* **2011**, *10*, 765–771.

[13] W. U. Huynh, J. J. Dittmer, A. P. Alivisatos, *Science (80-.).* **2002**, *295*, 2425–2427.

[14] Z. R. Tian, J. A. Voigt, J. Liu, B. Mckenzie, M. J. Mcdermott, M. A. Rodriguez, H. Konishi, H. Xu, *Nat. Mater.* **2003**, *2*, 821–826.

[15] L. Schmidt-Mende, J. L. MacManus-Driscoll, *Mater. Today* **2007**, *10*, 40–48.

[16] H. Jaffe, D. A. Berlincourt, *Proc. IEEE* **1965**, *53*, 1372–1386.

[17] S. M. Yu, *Nat. Nano.* **2012**, *7*, 343–344.

[18] S. Xu, Y. Qin, C. Xu, Y. Wei, R. Yang, Z. L. Wang, *Nat. Nano.* **2010**, *5*, 366–373.

[19] J. Briscoe, M. Stewart, M. Vopson, M. Cain, P. M. Weaver, S. Dunn, *Adv. Energy Mater.* **2012**, *2*, 1261–1268.

[20] J. Briscoe, N. Jalali, P. Woolliams, M. Stewart, P. M. Weaver, M. Cain, S. Dunn, *Energy Environ. Sci.* **2013**, *6*, 3035–3045.

[21] X. Wang, J. Song, J. Liu, Z. L. Wang, *Science (80-.).* **2007**, *316*, 102–105.

[22] S. Y. Yang, J. Seidel, S. J. Byrnes, P. Shafer, C.-H. Yang, M. D. Rossell, P. Yu, Y.-H. Chu, J. F. Scott, J. W. Ager, L. W. Martin, R. Ramesh, *Nat. Nano.* **2010**, *5*, 143–147.

[23] H. Huang, *Nat. Photon.* **2010**, *4*, 134–135.

[24] Y. Zheng, C. H. Woo, *J. Appl. Phys.* **2010**, *107*, 104120.

[25] A. B. Djurišić, Y. H. Leung, *Small* **2006**, *2*, 944–961.

[26] R. Könenkamp, R. C. Word, M. Godinez, *Nano Lett.* **2005**, *5*, 2005–2008.

[27] M. Law, L. E. Greene, J. C. Johnson, R. Saykally, P. Yang, *Nat. Mater.* **2005**, *4*, 455–459.

[28] D. Choi, K. Y. Lee, M.-J. Jin, S.-G. Ihn, S. Yun, X. Bulliard, W. Choi, S. Y. Lee, S.-W. Kim, J.-Y. Choi, J. M. Kim, Z. L. Wang, *Energy Environ. Sci.* **2011**, *4*, 4607–4613.

[29] C. Xu, X. Wang, Z. L. Wang, *J. Am. Chem. Soc.* **2009**, *131*, 5866–5872.

[30] Y. Yang, W. Guo, Y. Zhang, Y. Ding, X. Wang, Z. L. Wang, *Nano Lett.* **2011**, *11*, 4812–4817.

[31] C. Xu, Z. L. Wang, *Adv. Mater.* **2011**, *23*, 873–877.

[32] J. Briscoe, D. E. Gallardo, S. Hatch, V. Lesnyak, N. Gaponik, S. Dunn, *J. Mater. Chem.* **2011**, *21*, 2517–2523.

[33] B. Wei, K. Zheng, Y. Ji, Y. Zhang, Z. Zhang, X. Han, *Nano Lett.* **2012**, *12*, 4595–4599.

[34] R. Österbacka, C. P. An, X. M. Jiang, Z. V Vardeny, *Sci.* **2000**, *287* , 839–842.

[35] P. P. Boix, Y. H. Lee, F. Fabregat-Santiago, S. H. Im, I. Mora-Sero, J. Bisquert, S. Il Seok, *ACS Nano* **2011**, *6*, 873–880.

[36] R. Hamilton, C. G. Shuttle, B. O'Regan, T. C. Hammant, J. Nelson, J. R. Durrant, *J. Phys. Chem. Lett.* **2010**, *1*, 1432–1436.

[37] L. Wang, X. Tian, S. Yang, Z. Xu, W. Wang, X. Bai, *Appl. Phys. Lett.* **2012**, *100*, 163110.

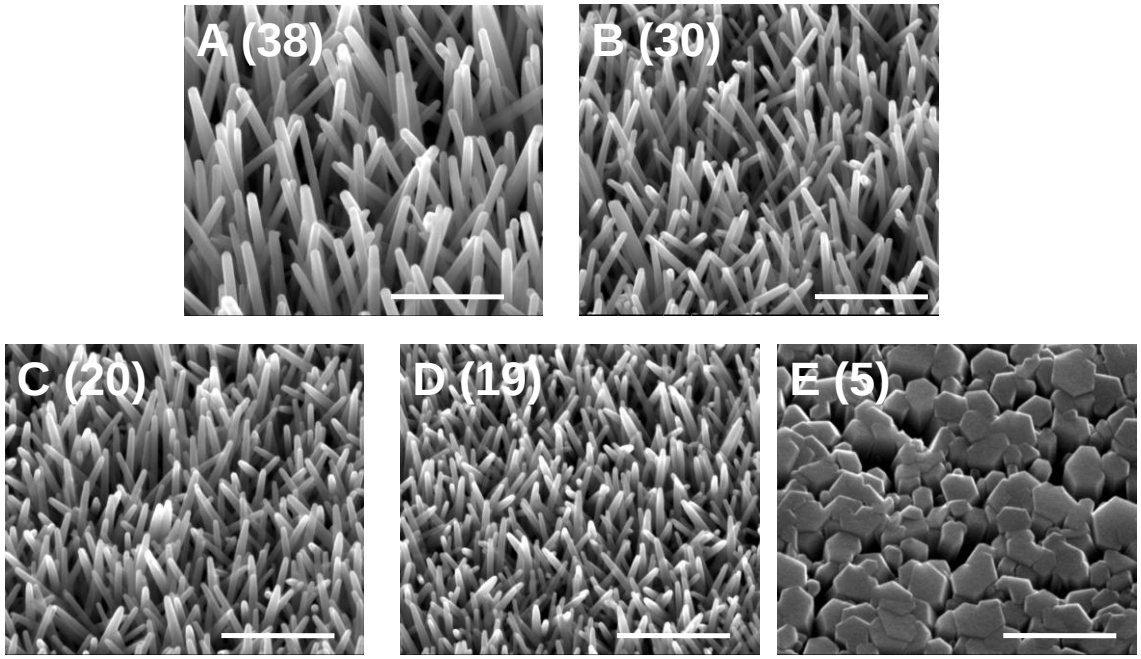

Figure 1. Cross sectional SEM images of ZnO(X) nanorods; each scale-bar corresponds to 1μm.

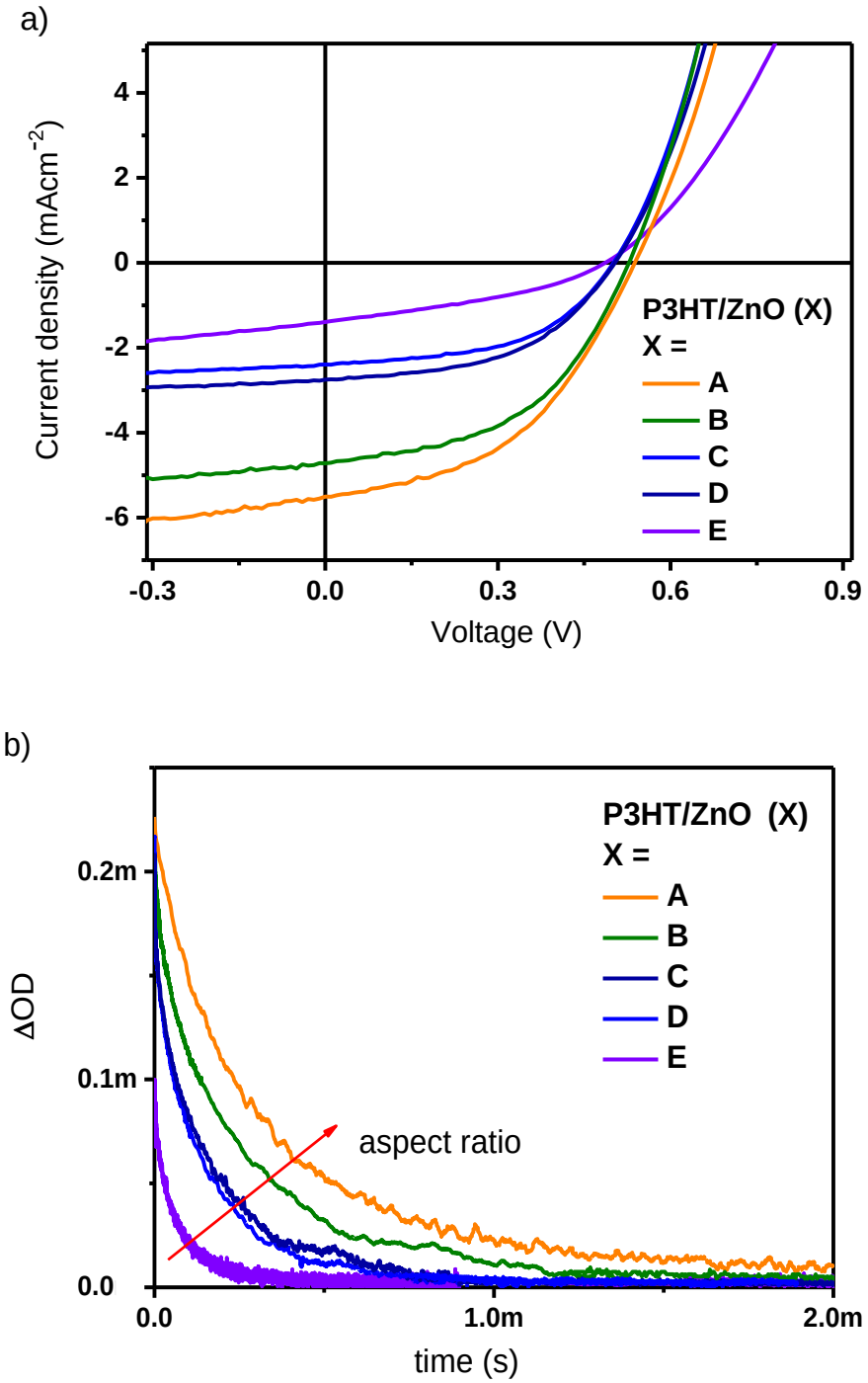

Figure 2 J-V curves (a) and transient absorption signals (b) of P3HT/ZnO(X) active layers with aspect ratios of A:38, B:30, C:20, D:19, E:5. Transient absorption data measured under N_2 atmosphere, probed at 980 nm and excited at 500 nm with an excitation intensity of 6 μJcm^{-2}. The y-axis (ΔOD) corresponds to charge photogeneration yield.

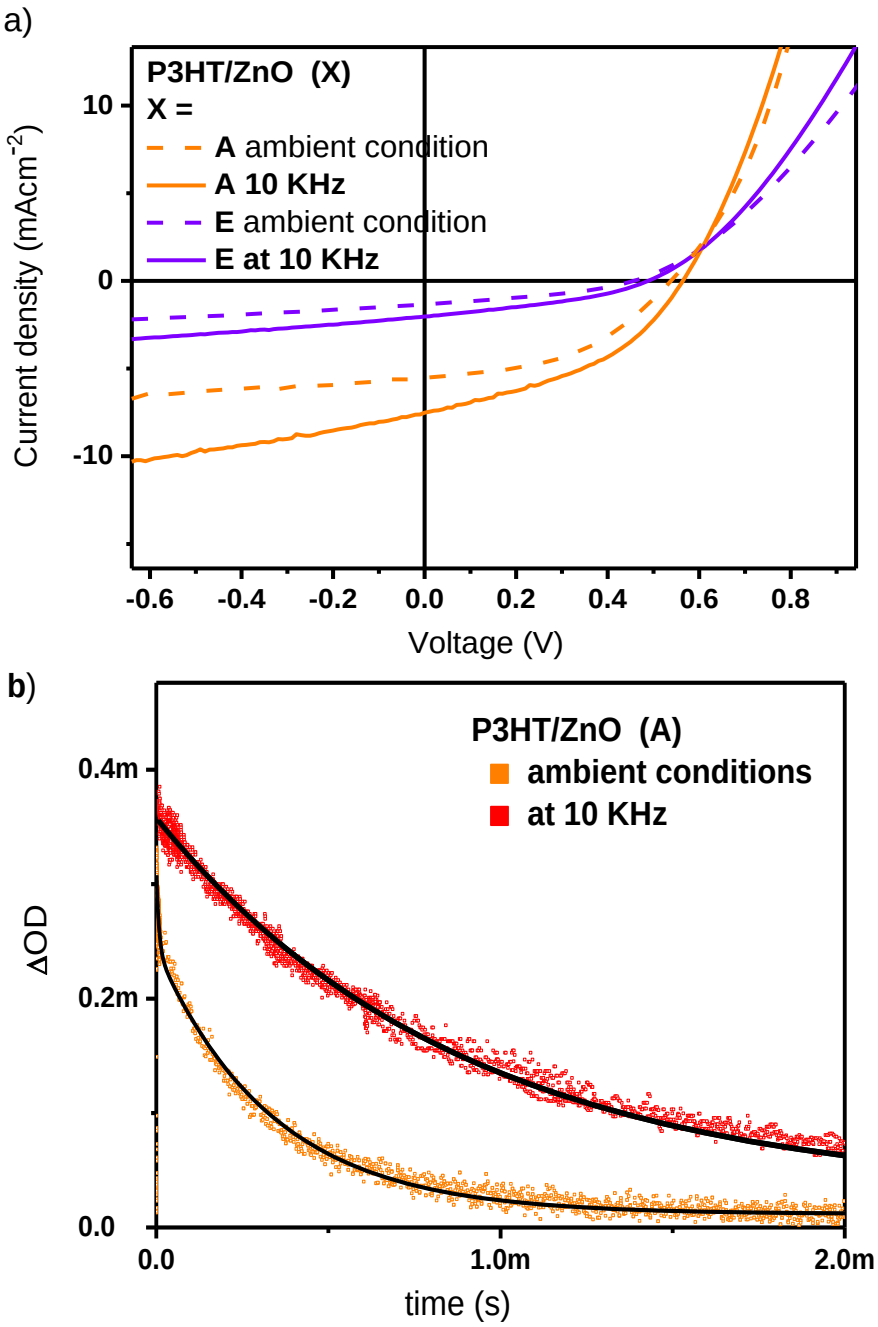

Figure 3. J-V curves of P3HT/ZnO(A) and P3HT/ZnO(E) devices (a) and transient absorption signals (b) of P3HT/ZnO(A) ± external frequency of 10 KHz at 75 dB. Transient absorption data measured under N_2 atmosphere, probed at 980 nm and excited at 500 nm with an excitation intensity of 6 μJcm^{-2}. The change in the y-axis indicates a change in the yield of photogenerated charges.

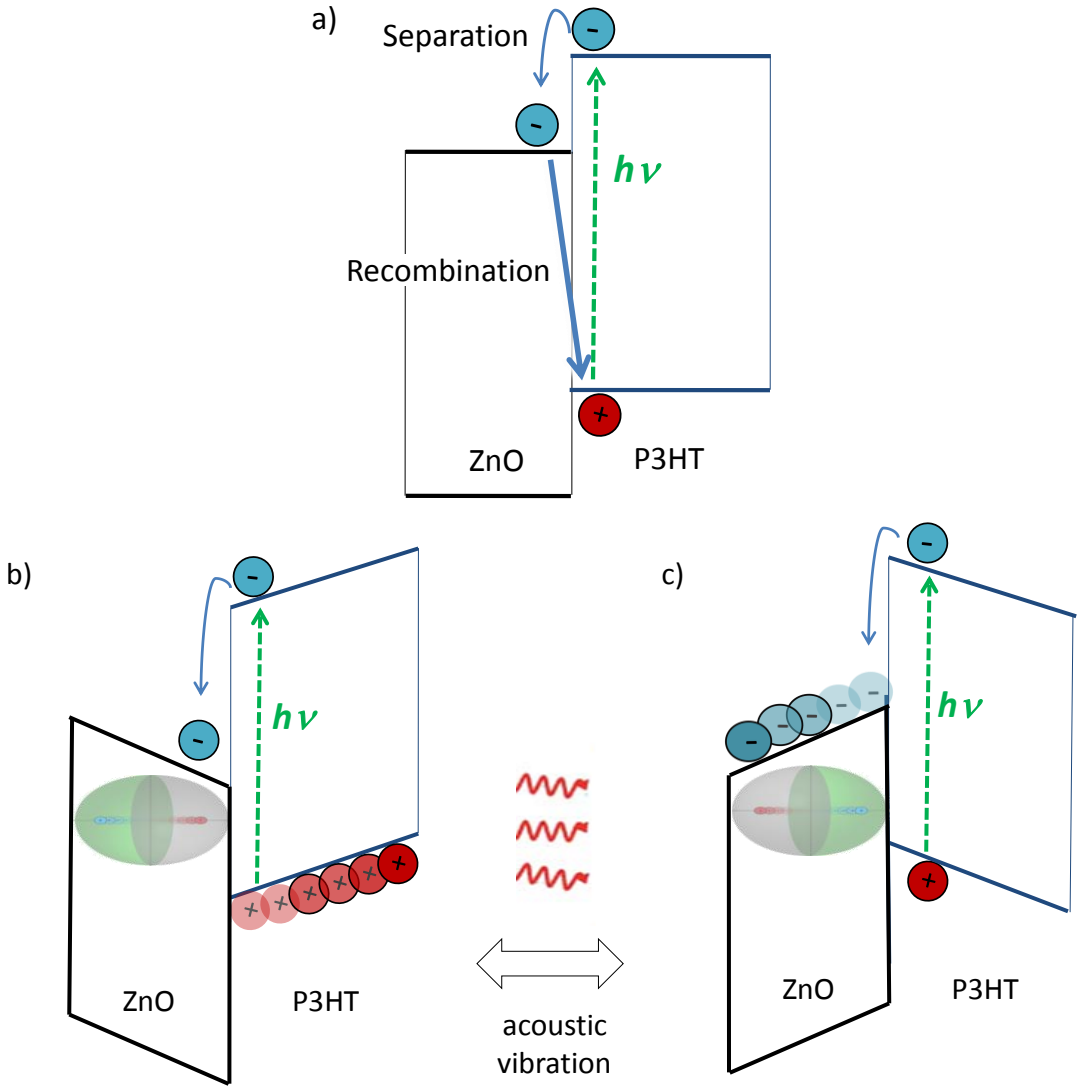

Figure 4. Schematic of P3HT/ZnO nanorod system illustrating the potential impact of an oscillating acoustic vibration upon photoinduced charge carrier dynamics. Illustrated are the dynamics in the absence of acoustic vibration (a) and in the presence of acoustic strains of opposite signs (b and c), illustrating the potential impact of strain-induced piezoelectric dipoles upon these charge carriers. For simplicity, the impact of space charge layers and band bending is neglected, as are charge transport processes to the device electrodes. The gradients of the conduction & valence band edges in (b) and (c) illustrate the impact of the piezoelectric ZnO polarisation upon these energy levels. In (b) the ZnO polarisation drives P3HT holes away from the interface. With the hole moved away from the junction, electrons are unable to cross it due to the energy barrier In (c), the opposite polarisation, ZnO electrons are driven from the surface and holes cannot cross the junction. In both cases, the net effect is to increase the spatial separation of electrons and holes, and so reduce recombination losses.

Submitted to ADVANCED MATERIALS

Acoustic vibrations are shown to enhance the photovoltaic efficiency of a P3HT/ZnO nanorod solar cell by up to 45%, correlated to a three-fold increase in charge carrier lifetime. This is assigned to the generation of piezoelectric dipoles in the ZnO nanorods, indicating that the efficiency of solar cells may be enhanced in the presence of ambient vibrations by the use of piezoelectric materials.

Keyword solar cell, piezoelectric, hybrid, zinc oxide, P3HT

S. Shoaee, J. Briscoe, J. R Durrant, S. Dunn*

Acoustic enhancement of polymer/ZnO nanorod photovoltaic device performance

ToC figure

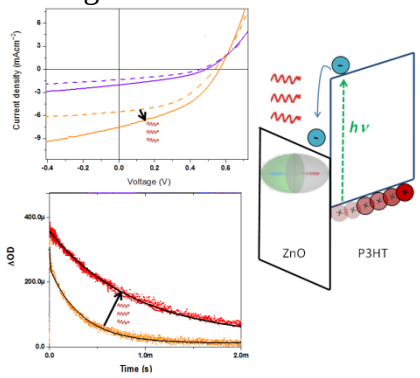

Supporting Information

for *Adv. Mater.*, DOI: 10.1002/adma.((please add manuscript number))

Acoustic enhancement of polymer/ZnO nanorod photovoltaic device performance

*Safa Shoaee, Joe Briscoe, James R Durrant and Steve Dunn**

Table S1 Summary of materials characterisation obtained for the films studied herein, including polaron lifetime and yields determined from transient absorption data, device photocurrent densities, photovoltage and device efficiency, all with and without applied vibration.

	ZnO(A)	ZnO(B)	ZnO(C)	ZnO(D)	ZnO(E)
Average length (μm)	2.7	1.4	1.1	0.8	1.4
Aspect ratio	38.1	29.8	19.8	18.8	5.3
Number density (μm^{-2})	40	50	75	105	25
Surface enhancement*	24	11	14	12	30
τ (s)	2.7×10^{-4}	1.78×10^{-4}	1.10×10^{-4}	9.8×10^{-5}	6×10^{-5}
τ_{VIB} (s)	8.8×10^{-4}	5.4×10^{-4}	1.8×10^{-4}	1.7×10^{-4}	1.15×10^{-4}
ΔOD (1 μs)	2.19×10^{-4}	2.04×10^{-4}	1.79×10^{-4}	1.83×10^{-4}	9×10^{-5}
ΔOD_{VIB} (1 μs)	3.56×10^{-4}	2.7×10^{-4}	2.26×10^{-4}	2.83×10^{-4}	2.08×10^{-4}
J_{SC} ($mAcm^{-2}$)	5.51	4.72	2.39	2.75	1.39
J_{SC-VIB} ($mAcm^{-2}$)	7.52	6.23	4.60	5.04	2.03
V_{OC} (V)	0.54	0.53	0.50	0.50	0.45
V_{OC-VIB} (V)	0.57	0.54	0.51	0.52	0.50
η %	1.35	1.21	0.82	0.86	0.24
η_{VIB} %	1.75	1.51	0.92	1.09	0.35

* Surface enhancement calculated by multiplying the average surface area of the rods by the number density. This does not account for fused rods, which may be particularly relevant for ZnO(E) which has a larger number of fused rods due to their large diameter (See Figure 1).

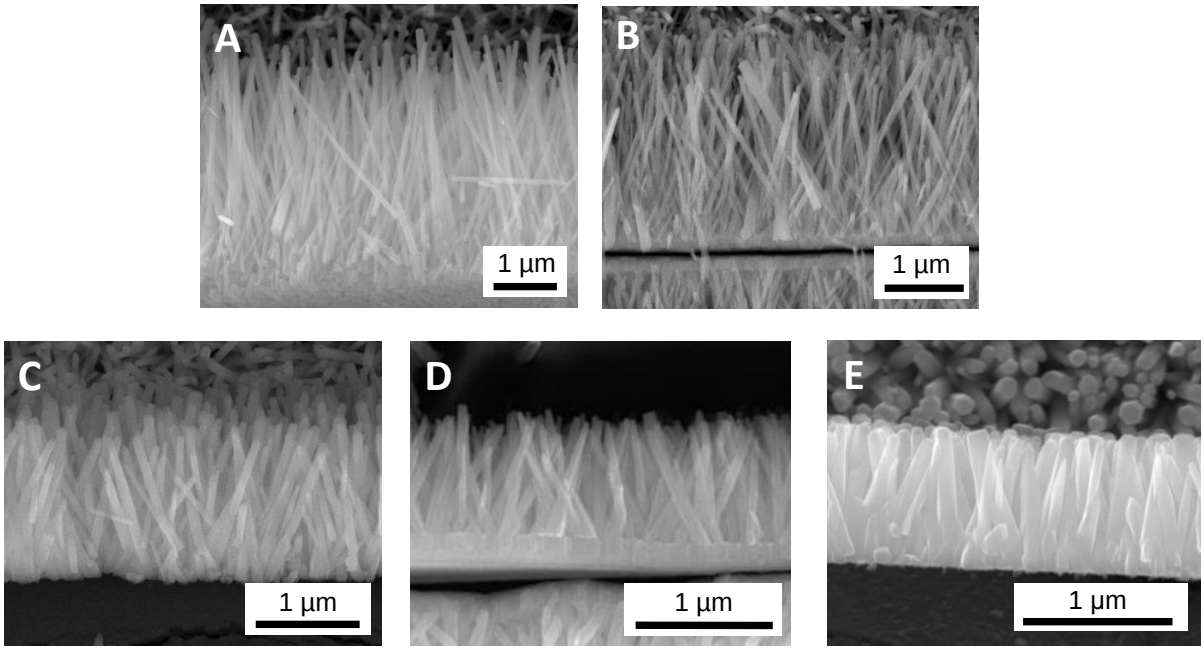

Figure S1. Cross-section SEM images of ZnO(X) used to measure average length and aspect ratio as shown in Table S1.

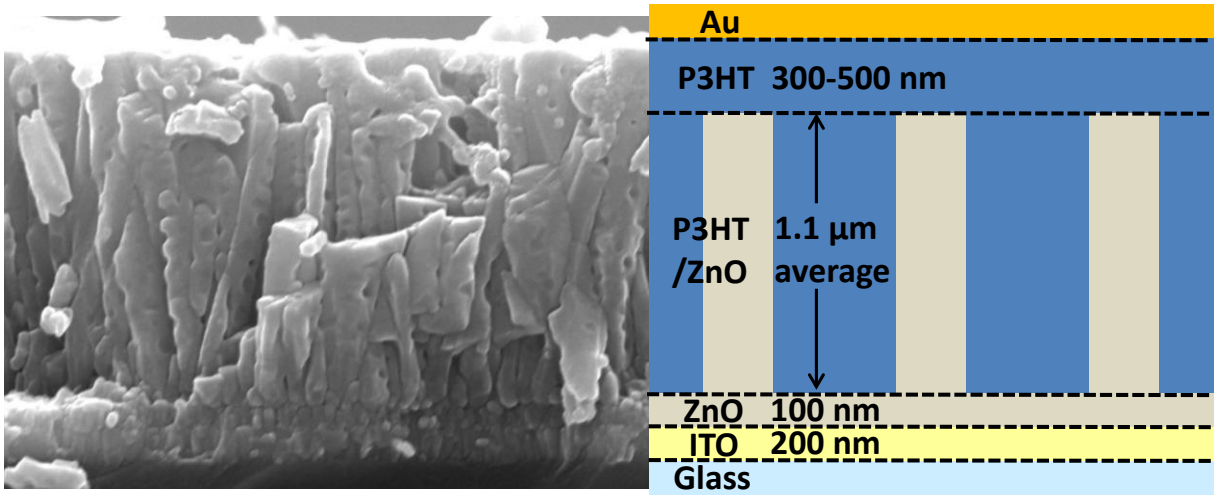

Figure S2. Example cross-section SEM image of P3HT/ZnO(C) with corresponding schematic showing thickness of each layer. It can be seen that the P3HT penetrates well between the ZnO nanorods so that their structure can only just be distinguished beneath the P3HT infill. Thus the P3HT/ZnO thickness in each case is equal to the length of the ZnO nanorods, and the P3HT/ZnO interface area is equal to the surface enhancement shown in Table S1. The thickness of P3HT layer above the ZnO nanorods varies due to the distribution of nanorod heights.

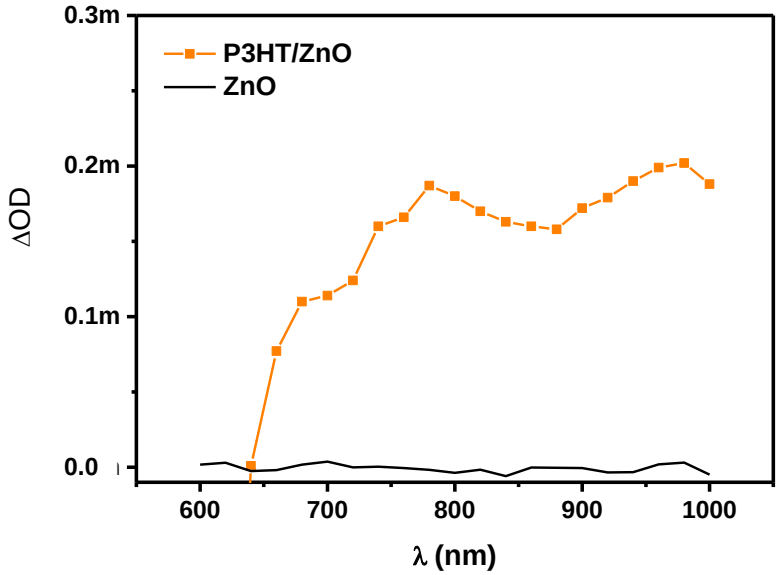

Figure S3. Transient absorption of ZnO and P3HT/ZnO(A) films at 1 μs. Data were taken at 1 μs, under nitrogen atmosphere, excited at 500 nm with an intensity of 6 μJcm^{-2}.

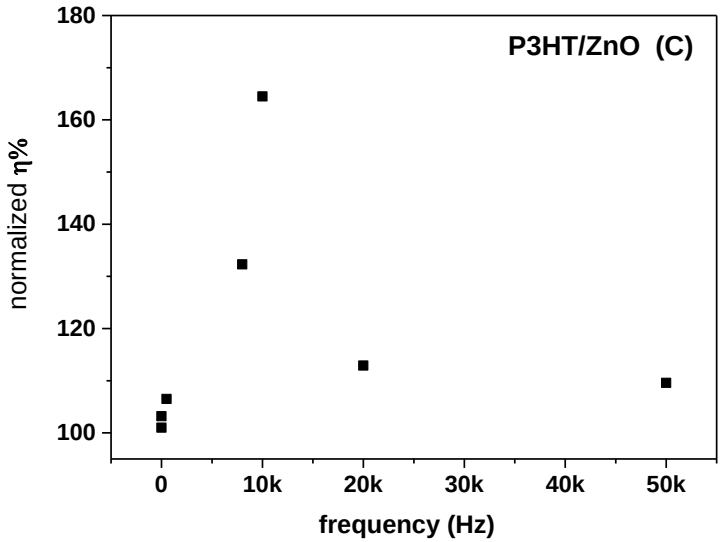

Figure S4. Frequency profile of P3HT/ZnO(C) device efficiency. The external vibration was applied at a fixed distance, through a loud speaker at 75 dB, with frequencies ranging between 1–50 kHz.

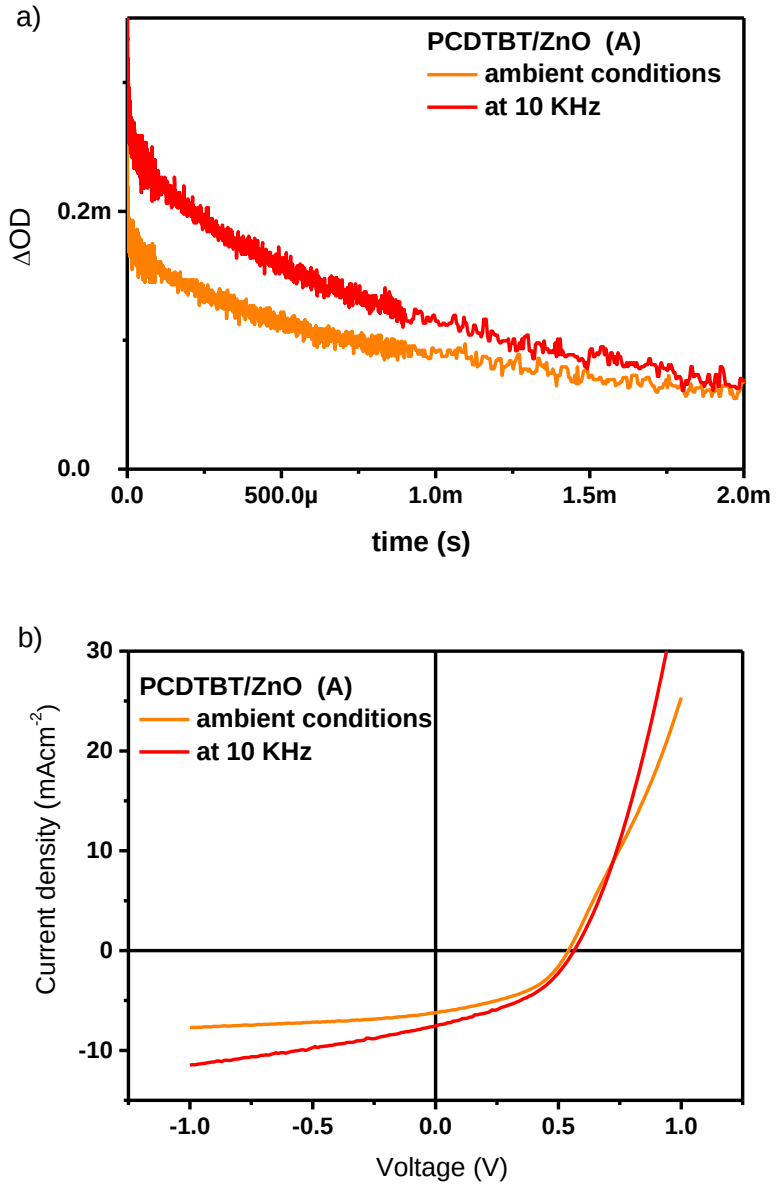

Figure S5. a) Transient absorption signals of PCDTBT/ZnO(A) film ± external frequency (10 kHz). Data were taken under nitrogen atmosphere, excited at 550 nm with an intensity of 6 μJcm^{-2}, probing PCDTBT^{+} at 980 nm, b) J-V curves of PCDTBT/ZnO(A) ± applied vibration at 75 dB at 1 sun.

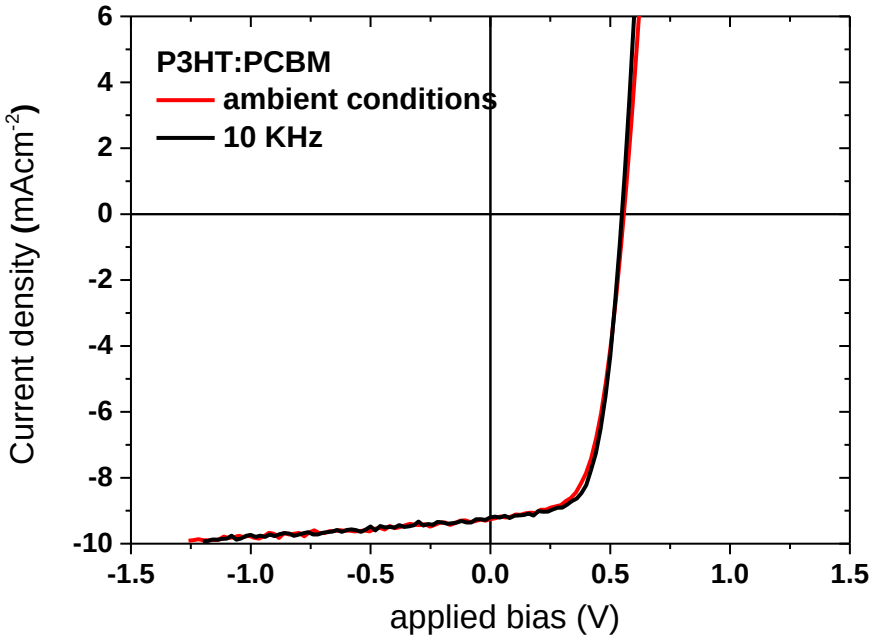

Figure S6. J-V curves of P3HT:PCBM ± applied vibration at 75 dB.

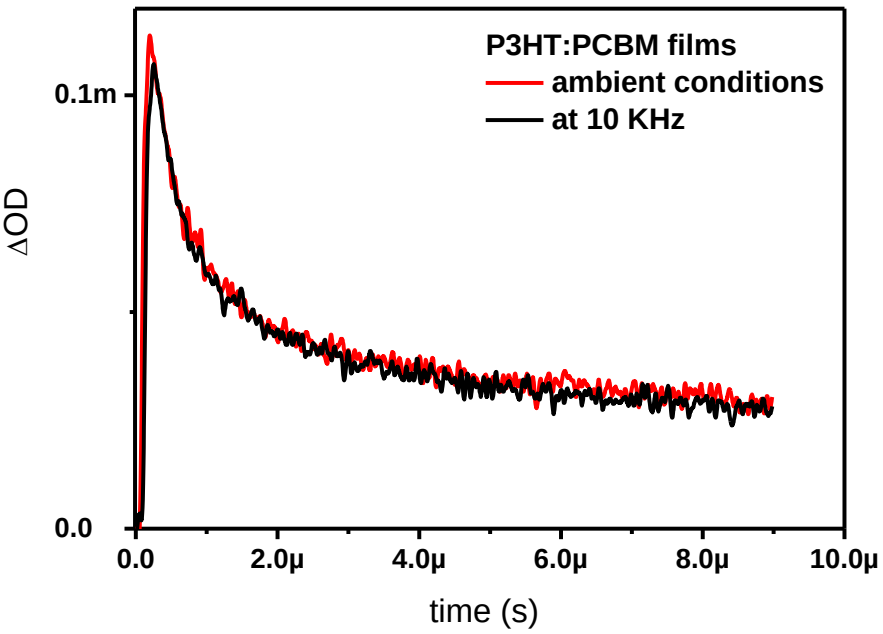

Figure S7. Transient absorption signals of P3HT:PCBM film ± external frequency (10 KHz). Data were taken under nitrogen atmosphere, excited at 500 nm with an intensity of 6 μJcm^{-2}, probing P3HT^{+} at 980 nm.

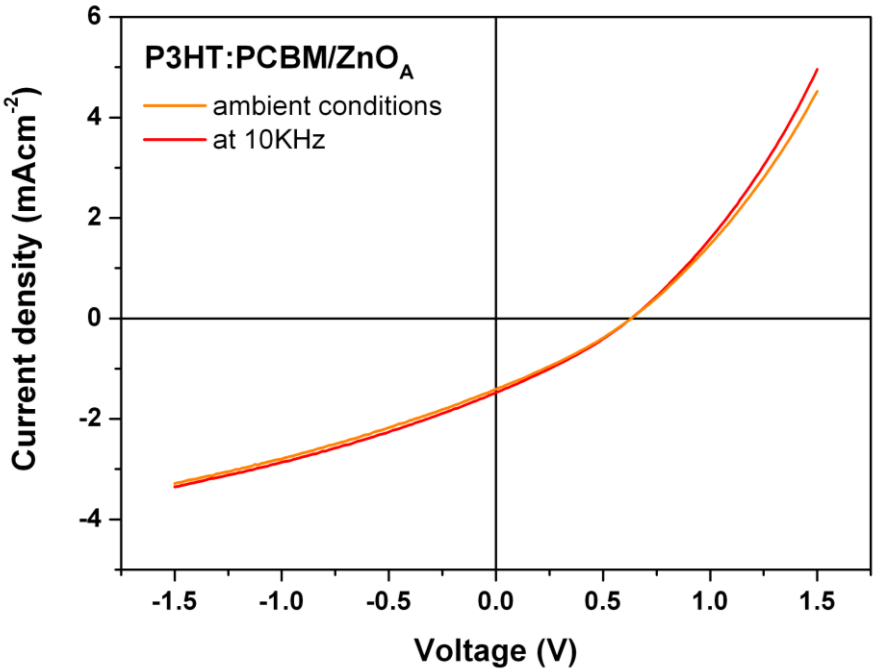

Figure S8. J-V curves of P3HT:PCBM on ZnO(A) ± applied vibration at 75 dB at 1 sun.

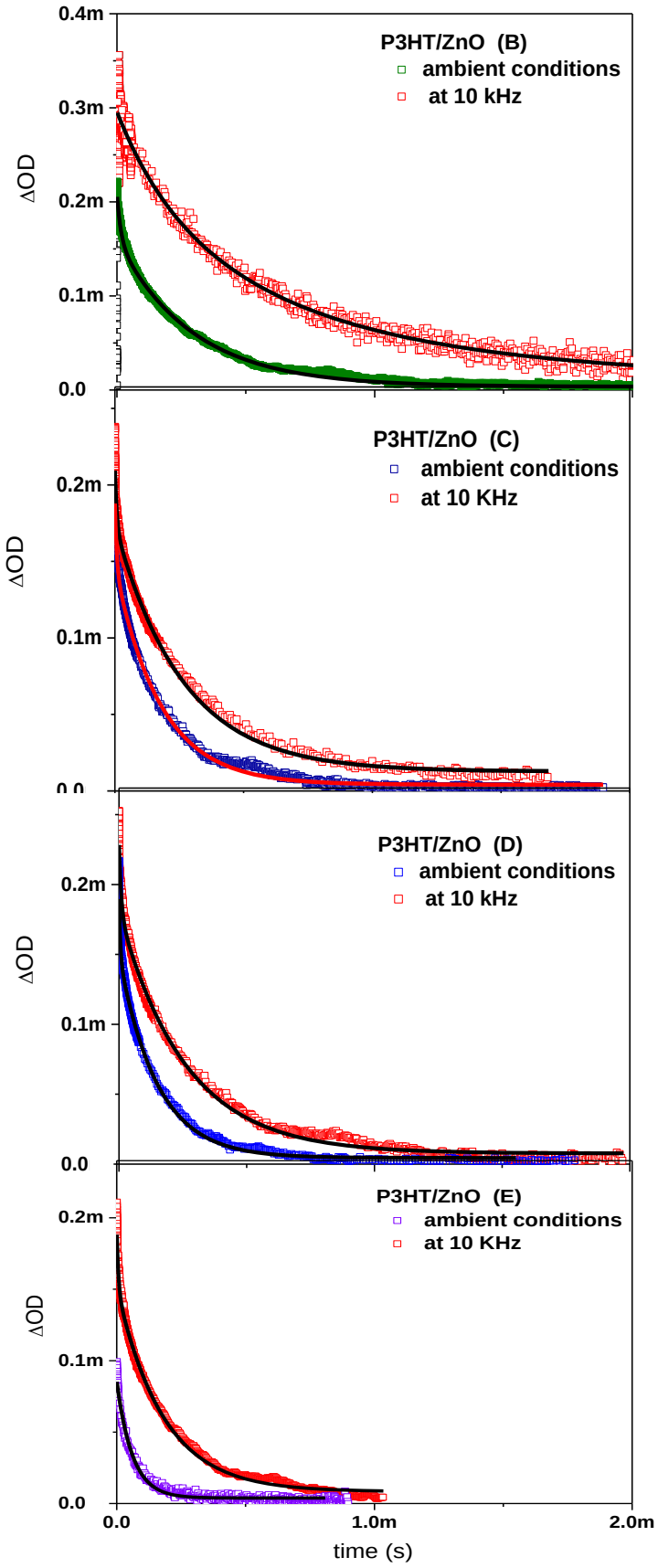

Figure S9. Transient absorption signals of P3HT/ZnO(X) films ± external frequency (at 10 kHz at 75 dB). Data were taken under nitrogen atmosphere, excited at 500 nm with an intensity of 6 μJcm^{-2}, probing P3HT^{+} at 980 nm.

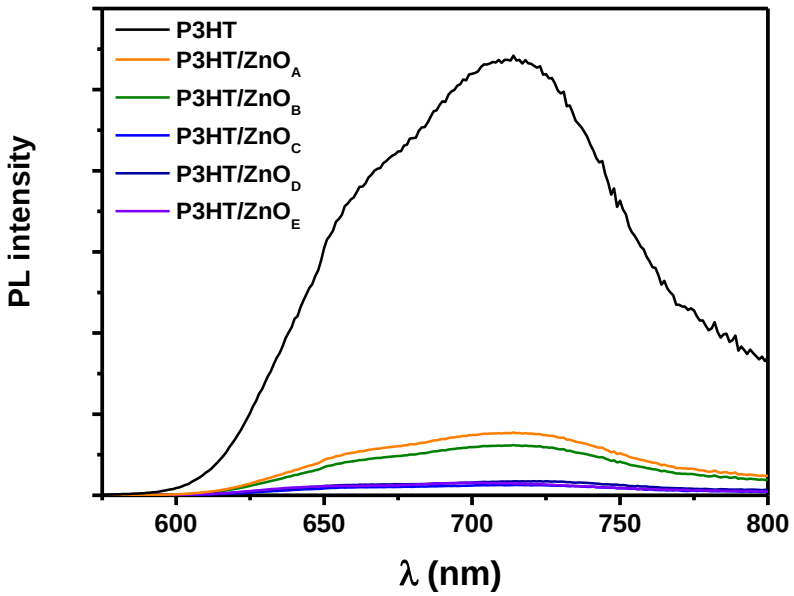

Figure S10. Photoluminescence spectra for P3HT and P3HT/ZnO(X) films, following excitation at 500 nm, allowing quantification of the extent of P3HT emission quenching in the P3HT/ZnO films relative to a neat P3HT film. In all cases the P3HT emission is quenched by over 90 %, which is in agreement with the intimate interface as seen in Figure S2. The slightly lower PL quenching for ZnO(A) and ZnO(B) may correlate with the lower number density of rods, indicated larger pores and a greater volume of P3HT not in direct contact with the ZnO rods and therefore not fully quenched.